Check for updates

Non-solvating, side-chain polymer electrolytes as lithium single-ion conductors: synthesis and ion transport characterization†

Jiacheng Liu, [ID] [a] Phillip D. Pickett, [ID] [b] Bumjun Park, [ID] [a] Sunil P. Upadhyay, [ID] [a] Sara V. Orski [ID] [b] and Jennifer L. Schaefer [ID] *[a]

Solid-state single-ion conducting polymer electrolytes have drawn considerable interest for secondary lithium batteries due to their potential for high electrochemical stability and safety, but applications are limited by their low ionic conductivities. Specifically, poly(ethylene oxide) (PEO) based electrolytes have the highest reported Li$^+$ conductivities for these materials; however, their potential is limited due to the ion transport mechanism being coupled to segmental relaxations of the cation solvating polymer chain. To investigate the potential of single-ion conducting polymer electrolytes lacking polar matrices, we synthesized three *para*-polyphenylene-based, side-chain polymer electrolytes with various pendent anion chemistries ($-SO_3^-$, $-PSI^-$, and $-TFSI^-$) with differing binding affinities to Li$^+$. Compared with the previously reported lithium poly(4-styrenesulfonyl(trifluoromethylsulfonyl)imide) (LiPSTFSI), the side-chain polymers showed at least 3 orders of magnitude higher conductivity with the same $-TFSI^-$ anion (6.7×10^{-6} S cm^{-1} compared with 1.2×10^{-10} S cm^{-1} at 150 °C). We found that the side-chain electrolyte showed a dielectric relaxation dominated transport mechanism through use of dielectric spectroscopy analysis. The conductivity is highly dependent on the charge delocalization and size of the pendent anion, which provides a pathway forward for the engineering of polymeric ion conductors for electrochemical applications.

[a]Department of Chemical and Biomolecular Engineering, University of Notre Dame, Notre Dame, IN, USA. E-mail: Jennifer.L.Schaefer.43@nd.edu
[b]Materials Science and Engineering Division, Material Measurement Laboratory, National Institute of Standards and Technology, Gaithersburg, MD, USA

†Electronic supplementary information (ESI) available. See DOI: 10.1039/c9py01035a

Introduction

As modern society's demand for personal electronic devices, robotics, and electrical vehicles increases, advanced energy storage devices with enhanced safety, energy density, and power density are of high interest. Lithium-ion batteries now comprise a major fraction of worldwide battery sales and offer energy densities that exceed other commercially available rechargeable battery chemistries such as nickel metal hydride and nickel cadmium.[1] However, the organic liquid electrolyte used in commercialized Li-ion batteries is inherently unsafe because of its flammability.[2] Additionally, this liquid electrolyte is reactive with lithium metal anodes that offer higher energy densities compared to the commercialized Li-ion anodes.[3] Therefore, for several decades there has been world-wide interest in developing a lithium conducting polymer elec-trolyte that offers improved thermal and chemical stability against the lithium metal anode for rechargeable batteries.[4]

Conventional polymer electrolytes are dual-ion conductors where the inactive anion is more mobile than the active lithium cation. As a result, deleterious ion concentration gradients develop in the electrolyte during battery operation. This leads to the accumulation of anions near the electrode–electrolyte surface during cell cycling. The effects of this concentration polarization include higher voltage loss and undesired side reactions that increase interfacial impedance and decrease cell lifetime.[5–7] Concentration polarization within the electrolyte may be mitigated by fixing the anion to the polymer matrix to create a single-ion conductor. Single-ion conducting polymer electrolytes allow for higher electrochemical stability, lower impedance, and higher current densities achieved by electrolytes of lower total ionic conductivity.[6–8] Considerable attention has been paid to single-ion conducting lithium polymer electrolytes based on poly(ethylene oxide) (PEO), but the conductivity of these electrolytes is known to be limited by the dissociability of the ion pair and the segmental mobility of the matrix.[9,10] Along these lines, copolymers containing lithium poly(4-styrenesulfonyl(trifluoromethylsulfonyl)imide) (LiPSTFSI) and PEO have been of interest because the –STFSI anion has a more delocalized charge than the simple carboxy-

late and sulfonate groups and is produced *via* a straightforward derivatization of the sulfonate anion.[8,11–15] Higher conductivities have been demonstrated with an even more delocalized tethered anion, but its synthesis is challenging.[8] Yet, despite decades of work to tailor various aspects of poly (ethylene oxide) based single-ion conducting polymer electrolytes, their conductivity is still inadequate for most batteries operating at ambient temperatures.

Recently, researchers have investigated ion-containing polymers neutralized by various metal ions wherein there is not a polar matrix for cation solvation as non-solvating single-ion conducting polymer electrolytes; reports on this class of electrolytes are still rare. Polymers of this type that have been investigated in the context of electrolytes include polyethylenes with directly pendant carboxylate or sulfonate ionic groups, along with LiPSTFSI homopolymers.[12,16–19] Molecular dynamics simulations have intriguingly shown that two ion transport modes are possible: (1) direct hopping within the ionic aggregates, and (2) relaxation related ion pair rearrangements.[20,21] In either case, the cation is not solvated by the matrix but rather coordinated with anionic groups during the transport. It is not yet known if these conduction mechanisms can achieve higher cation conductivities than what is possible with the PEO-based single-ion conductors. A recent study has shown that a polyethylene type non-solvating electrolyte with sulfonate and metal ion pairs exhibits very low and Arrhenius temperature-dependent ionic conductivity, indicating the potential for decoupling of conductivity from mechanical properties.[22] However, non-solvating polymer electrolytes containing ion pairs with lower binding affinities have not been widely studied yet, even though it is intuitive to expect them to provide higher conductivity. As polymerized ionic liquids (PILs) contain ion pairs with much lower binding energy, lessons learned from the study of ion transport in those ionic polymers may be valuable here.

PILs have drawn attention for potential application as solid state electrolytes in batteries and fuel cells, gas separation membranes, and sensors.[23] They typically contain a high concentration of organic ion pairs with low charge density, in comparison to metal ions, and therefore their counter-ion transport rate is often correlated with the relaxation of ion pairs that is influenced by the segmental flexibility (related to the glass transition, T_g) and dielectric constant.[24–26] The coupling of ion and polymer relaxation is not absolute, however, with decoupling of these parameters observed for various PILs, typically at temperatures approaching the glass transition.[27] Recent molecular dynamics simulations on these materials predict that ion mobility may be increased while maximizing decoupling and minimizing T_g by creating systems with aggregated ionic domains, large bound ions, and small mobile ions.[28] The aggregated ions could be achieved by use of a noninteracting polymer backbone and placement of the tethered ions on side-chains.

Inspired by previous efforts in non-solvating, single-ion conducting polymer electrolytes for metal-ion batteries as well as the polymerized ionic liquids field, we report on the synthesis and characterization of a new family of side-chain, lithium single-ion conducting polymer electrolytes without a polar matrix. The polymers are prepared *via* the Negishi coupling polymerization of ionically functionalized *p*-phenylene monomers to produce a rigid, non-interacting poly(*p*-phenylene) backbone. The anions have enhanced flexibility and configurational freedom due to their location on the terminal end of alkyl side-chains. In addition, the chemistry of the anionic group is altered to investigate its effect on lithium cation transport. We find that the ion transport process is strongly coupled to the dielectric relaxation. More dissociable tethered anions and presence of the side-chain are both correlated with enhanced dielectric relaxation and higher lithium conductivity.

Materials and methods‡

Materials

2,5-Dichlorophenol, 1,10-dibromodecane (98%), sodium sulfite (≥98%), potassium carbonate (≥99%), potassium iodide (≥99%), thionyl chloride (≥99%), trimethylamine (>99.5%), benzyltriethylammonium bromide (BzNEt₃Br, 99%), lithium hydride (95%), benzensulfonamide (>98%), triphenylphosphine (P(Ph)₃, 99%), bipyridine (bpy, ≥99%), acetone (ACS grade), ethanol (ACS grade), *N,N*-dimethylformamide (DMF, anhydrous, 99.8%), *N,N*-dimethylacetamide (DMAc, anhydrous), tetrahydrofuran (THF, anhydrous, ≥99.9%), dichloromethane (DCM, ≥99.5%), and hydrochloric acid (37 mass %) were obtained from Sigma-Aldrich. Zinc powder was obtained from Alfa Aesar. Trifluoromethanesulfonamide (>98%) was purchased from TCI Chemicals. All materials were used as received. The Spectra/Por® 7 dialysis tubing with MWCO 1000 was obtained from Spectrum Laboratories. A Milli-Q system was used to generate deionized (DI) water (18 MΩ).

Nuclear magnetic resonance (NMR)

¹H, ¹³C, and ¹⁹F NMR spectra were acquired on a Bruker AVANCE III HD 400 Nanobay spectrometer.

Attenuated total reflection- Fourier transformation infrared spectroscopy (ATR-FTIR)

The ATR-FTIR data was recorded on a Jasco FT/IR-6300 spectrometer equipped with a ZnSe ATR crystal. The spectra were collected from 4000 cm⁻¹ to 650 cm⁻¹ at 4 cm⁻¹ resolution with 64 scans.

Differential scanning calorimetry (DSC)

The thermal transitions of various polymer electrolytes were profiled by differential scanning calorimetry (DSC). A DSC Q2000 (TA Instruments) was used at a heating/cooling rate of

‡Certain equipment, instruments or materials are identified in this paper in order to adequately specify the experimental details. Such identification does not imply recommendation by the National Institute of Standards and Technology nor does it imply the materials are necessarily the best available for the purpose.

10 °C min^{-1} with a N$_2$ purge of 50 mL min^{-1}. Samples were first heated to 200 °C (300 °C for oligo-**2**) and maintained at that temperature for 10 min to remove thermal history. Data is reported for the cooling and second heating scan.

Gel permeation chromatography (GPC)

The poly(lithium ((10-(2,5-dichlorophenoxy)decyl)sulfonyl)((tri-fluoromethyl)sulfonyl)imide) (poly-**6**), poly(lithium ((10-(2,5-dichlorophenoxy)decyl)sulfonyl)(phenylsulfonyl)imide) (poly-**7**), and LiPSTFSI were characterized by a DMF mobile phase GPC. It was performed with a Waters 1515 Isocratic HPLC Pump equipped with a Waters 717 Autosampler, Waters 2487 Dual Wavelength Absorbance Detector (264 nm), and Waters 2414 Refractive Index Detector (30 °C) in series with Agilent PolarGel mixed-bed columns at 50 °C (two PL PolarGel-M, 7.5 mm × 300 mm, in series with a PL PolarGel-M guard column). The GPC instrument was interfaced using Waters Breeze v 3.30 software. The eluent used was 0.1 mol L^{-1} LiCl in dimethylformamide at a flow rate of 0.5 mL min^{-1}. Apparent molecular mass and molecular mass distributions were determined using poly(ethylene oxide) calibration standards.

The poly(lithium 10-(2,5-dichlorophenoxy)decane-1-sulfonate) (oligo-**2**) was characterized by an aqueous phase eluent (1 : 4 acetonitrile : water (volume fraction) with 0.2 M LiBr) on the same GPC system described above. The stationary phase was a series of three Tosoh TSKGel SuperAW columns (1× SuperAW guard, 1× SuperAW3000, and 1× SuperAW4000) at 30 °C. The eluent flow rate is 0.3 mL min^{-1}. The apparent molecular mass and molecular mass distribution was calculated based on poly(ethylene oxide) calibration standards.

Dielectric spectroscopy

Dielectric spectroscopy was performed on a Novocontrol Broadband spectrometer equipped with an alpha-A high performance frequency analyzer and Quatro temperature control system with a cryostat. For each poly-**6** and poly-**7**, a solution of the sample in DMF was cast on top of the electrode. Then a glass fiber spacer was applied to maintain a constant (50 μm) sample thickness. After 24 h of drying under a heat lamp, the sample was further dried in a vacuum oven at 180 °C to completely remove any residual solvent. Then, the sample was heated to 180 °C while a force was applied on the top electrode for 1 h to allow for a smooth contact and the thickness to equilibrate at 50 μm. The poly-**2** was measured as a pressed powder after a similar drying procedure. Dielectric data was collected in a frequency range from 0.01 Hz to 3 × 10^6 Hz and at an AC voltage of 0.3 V upon cooling. DC conductivity was determined by the plateau value of the real conductivity-frequency spectrum; error bars corresponding to one standard deviation are smaller than the symbol size.[29]

Synthesis of lithium poly(4-styrenesulfonyl(trifluoromethylsulfonyl)imide) (LiPSTFSI)

Lithium poly(4-styrenesulfonyl(trifluoromethylsulfonyl)imide) (LiPSTFSI) was synthesized according to a previously reported procedure followed by lithium-ion exchange by dialysis.[13]

Synthesis of 2-((10-bromodecyl)oxy)-1,4-dichlorobenzene (1)

2,5-Dichlorophenol (10 g, 61.3 mmol), 1,10-dibromodecane (55 g, 183.3 mmol), potassium carbonate (21 g, 152.2 mmol), potassium iodide (1.25 g, 7.7 mmol), and acetone (320 mL) were loaded into a round-bottom flask equipped with a magnetic stirrer bar. The mixture was refluxed under stirring for 12 h. After reaction, inorganic precipitates were filtered off, and then the solvent was evaporated under reduced pressure. The organic-oily mixture was added to cold methanol slowly, and the precipitate was collected. The product in the form of white powder was isolated by column chromatography (SiO$_2$, hexane). Yield: 15.46 g (66.0%).

^{1}H NMR (400 MHz, DMSO-d_6) δ 7.42 (dd, J = 8.5, 2.1 Hz, 1H), 7.21 (d, J = 2.3 Hz, 1H), 6.99 (ddd, J = 8.5, 2.3, 1.4 Hz, 1H), 4.06 (t, J = 6.4 Hz, 2H), 3.50 (td, J = 6.7, 1.7 Hz, 2H), 1.90–1.62 (m, 4H), 1.52–1.07 (m, 12H).

^{13}C NMR (101 MHz, DMSO-d_6) δ 154.65, 132.42, 130.77, 121.00, 120.21, 113.97, 68.97, 35.14, 32.26, 28.87, 28.80, 28.57, 28.35, 28.10, 27.54, 25.34.

Synthesis of sodium 10-(2,5-dichlorophenoxy)decane-1-sulfonate (2)

To a round bottom flask equipped with a magnetic stir bar, **1** (12 g, 31.4 mmol), sodium sulfite (9.9 g, 78.5 mmol), benzyltri-ethylammonium bromide (0.43 g, 1.58 mmol), and ethanol/water (88 mL, 1 : 1) were added. The mixture was refluxed at 95 °C for 24 h. Precipitate solid was hot filtered. Then the filtrate was allowed to cool down at room temperature for 12 h. The resulting mixture was filtered again. The solids were then stirred rigorously in dichloromethane (100 mL) and filtered to remove any unreacted organic precursor. A flakey, white product was obtained by recrystallization from water and subsequently dried in a vacuum oven for 12 h at 80 °C. Yield: 10.61 g (85.7%).

^{1}H NMR (400 MHz, DMSO-d_6) δ 7.44 (d, J = 8.5 Hz, 1H), 7.23 (d, J = 2.3 Hz, 1H), 7.00 (dd, J = 8.5, 2.3 Hz, 1H), 4.07 (t, J = 6.4 Hz, 2H), 2.45–2.10 (m, 2H), 1.72 (p, J = 6.5 Hz, 2H), 1.63–1.05 (m, 14H).

^{13}C NMR (101 MHz, DMSO-d_6) δ 154.68, 132.44, 130.81, 121.03, 120.22, 114.03, 69.03, 51.56, 29.02, 28.96, 28.93, 28.68, 28.50, 28.38, 25.39, 25.14.

Synthesis of 10-(2,5-dichlorophenoxy)decane-1-sulfonyl chloride (3)

In a glove box under argon atmosphere, **2** (7 g, 17.3 mmol), anhydrous THF (55 mL), and a catalytic amount of DMF was added to a dry round bottom flask. Then the flask was sealed and transferred to the Schlenk line, operating with dry nitrogen flow. The mixture was cooled to 4 °C with an ice/water bath, after which thionyl chloride (10.3 g, 86.3 mmol) was added slowly *via* syringe. The reaction was stirred at 4 °C for 1 h and then overnight at room temperature. After the reaction, the reaction mixture was poured into an ice/water (400 mL) mixture to quench the excess thionyl chloride. Then, the product was extracted from the aqueous mixture with di-

chloromethane (3 × 50 mL). The combined organic phase was washed with water (3 × 20 mL) and dried with anhydrous magnesium sulfate. After evaporating the solvent under reduced pressure, the resulting product was recrystallized from hexane. A colorless crystalline product was obtained. Yield: 6.11 g (88.0%).

^{1}H NMR (400 MHz, THF-d_8) δ 7.35 (d, J = 8.4 Hz, 1H), 7.11 (d, J = 2.3 Hz, 1H), 6.94 (dd, J = 8.4, 2.3 Hz, 1H), 4.08 (t, J = 6.4 Hz, 2H), 4.01–3.88 (m, 2H), 2.02 (tt, J = 7.8, 6.4 Hz, 2H), 1.93–1.79 (m, 2H), 1.64–1.22 (m, 12H).

^{13}C NMR (101 MHz, THF-d_8) δ 156.11, 133.64, 131.31, 121.85, 121.48, 114.36, 69.83, 65.56, 30.17, 29.97, 29.69, 29.65, 28.15, 26.67, 25.22.

Synthesis of triethyammonium ((10-(2,5-dichlorophenoxy)decyl)sulfonyl)((trifluoromethyl)sulfonyl)imide (4)

Trifluoromethanesulfonamide (2.27 g, 15.2 mmol), triethylamine (4.61 g, 45.6 mmol), and anhydrous THF (11 mL) were loaded into a dry round bottom flask with a magnetic stir bar in an argon glovebox. Then the flask was transferred to the Schlenk line, operating with dry nitrogen flow, and cooled to 4 °C. **3** (6.1 g, 15.2 mmol) was dissolved in anhydrous THF (20 mL) separately and then added to the above mixture dropwise. The reaction proceeded at 4 °C for 1 h and room temperature overnight. After reaction, inorganic precipitates were filtered off, and solvent was evaporated from the filtrate. The resulting oil was redissolved in DCM (100 mL). DCM solution was washed with water (3 × 30 mL), dried over anhydrous magnesium sulfate, and concentrated under reduced pressure. After further drying in a vacuum oven at 60 °C for 12 h, a yellowish, oily product was afforded. Yield: 8.82 g (94.2%).

^{1}H NMR (400 MHz, DMSO-d_6) δ 8.86 (s, 1H), 7.43 (d, J = 8.5 Hz, 1H), 7.22 (d, J = 2.4 Hz, 1H), 6.99 (dd, J = 8.4, 2.3 Hz, 1H), 4.06 (t, J = 6.4 Hz, 2H), 3.10 (q, J = 7.4 Hz, 6H), 3.00–2.85 (m, 2H), 1.81–1.55 (m, 4H), 1.47–1.21 (m, 12H), 1.17 (t, J = 7.3 Hz, 9H).

^{13}C NMR (101 MHz, DMSO-d_6) δ 154.68, 132.44, 130.79, 120.16, 121.01, 120.23, 118.55, 114.01, 69.02, 54.51, 45.77, 28.93, 28.77, 28.68, 28.63, 28.37, 27.76, 25.36, 23.69, 8.64.

^{19}F NMR (376 MHz, DMSO-d_6) δ −77.54.

Synthesis of triethyammonium ((10-(2,5-dichlorophenoxy)decyl)sulfonyl)(phenylsulfonyl)imide (5)

The synthesis procedure was the same as for **4** except that benzenesulfonamide was used in place of trifluoromethanesulfonamide. A yellowish, oily product was obtained. Yield: 4.5 g (94.1%).

^{1}H NMR (400 MHz, DMSO-d_6) δ 8.85 (s, 1H), 7.78–7.69 (m, 2H), 7.48–7.34 (m, 4H), 7.24 (d, J = 2.3 Hz, 1H), 7.01 (dd, J = 8.5, 2.3 Hz, 1H), 4.08 (t, J = 6.4 Hz, 2H), 3.09 (q, J = 7.3 Hz, 6H), 2.91–2.82 (m, 2H), 1.79–1.67 (m, 2H), 1.66–1.52 (m, 2H), 1.49–1.21 (m, 12H), 1.17 (t, J = 7.3 Hz, 9H).

^{13}C NMR (101 MHz, DMSO-d_6) δ 154.67, 146.85, 132.43, 130.79, 129.85, 127.77, 126.19, 121.02, 120.22, 114.02, 69.02, 54.02, 45.75, 28.96, 28.83, 28.78, 28.65, 28.37, 28.02, 25.37, 23.89, 8.63.

Synthesis of lithium ((10-(2,5-dichlorophenoxy)decyl)sulfonyl)((trifluoromethyl)sulfonyl)imide (6)

A suspension of lithium hydride (0.23 g, 28.9 mmol) in anhydrous THF (20 mL) was cooled to 4 °C with an ice/water bath under nitrogen atmosphere. Then a solution of compound **4** (8.8 g, 14.3 mmol) in anhydrous THF (15 mL) was added to the above suspension dropwise. The reaction was allowed to proceed at room temperature for 2 h. Then, the mixture was filtered to remove excess lithium hydride, and the solvent was evaporated off under reduced pressure. The resulting yellowish oil was stirred in chloroform (30 mL) to remove unreacted precursors, then the chloroform was decanted. After drying under vacuum at 80 °C for 24 h, a white powdery product was obtained. Yield: 6.64 g (88.9%).

^{1}H NMR (400 MHz, DMSO-d_6) δ 7.43 (d, J = 8.5 Hz, 1H), 7.22 (d, J = 2.4 Hz, 1H), 6.99 (dd, J = 8.5, 2.3 Hz, 1H), 4.06 (t, J = 6.4 Hz, 2H), 2.97–2.89 (m, 2H), 1.80–1.58 (m, 4H), 1.51–1.09 (m, 12H).

^{13}C NMR (101 MHz, DMSO-d_6) δ 154.70, 132.46, 130.81, 121.03, 120.25, 120.17, 118.56, 114.04, 69.04, 54.53, 40.15, 39.94, 39.73, 39.52, 39.31, 39.10, 38.89, 28.94, 28.78, 28.69, 28.65, 28.38, 27.77, 25.38, 23.70.

^{19}F NMR (376 MHz, DMSO-d_6) δ −77.52.

Synthesis of lithium ((10-(2,5-dichlorophenoxy)decyl)sulfonyl)(phenylsulfonyl)imide (7)

The procedure is the same as for **6** except that **5** was used as the precursor. A yellowish oily product was obtained. Yield: 2.5 g (65.61%).

^{1}H NMR (400 MHz, DMSO-d_6) δ 7.78–7.68 (m, 2H), 7.47–7.34 (m, 4H), 7.23 (d, J = 2.4 Hz, 1H), 7.00 (dd, J = 8.5, 2.3 Hz, 1H), 4.07 (t, J = 6.4 Hz, 2H), 2.90–2.81 (m, 2H), 1.81–1.66 (m, 2H), 1.65–1.51 (m, 2H), 1.50–1.11 (m, 12H).

^{13}C NMR (101 MHz, DMSO-d_6) δ 154.70, 146.92, 132.46, 130.82, 129.85, 127.79, 126.22, 121.05, 120.25, 114.04, 69.05, 54.05, 29.00, 28.86, 28.82, 28.68, 28.40, 28.05, 25.40, 23.92.

General procedure for polymer synthesis

The Negishi coupling polymerization was performed in an argon glove box and all the apparatus involved was dried. Anhydrous DMAc was first subjected to freeze–pump–thaw three times to remove oxygen. The monomer, nickel chloride (0.1 equiv.), triphenylphosphine (0.4 equiv.), bipyridine, (0.1 equiv.), zinc (3 equiv.), and DMAc (4.5 mL) were loaded into a round bottom flask. The mixture was first heated up to 50 °C and stirred for 1 h. Then the reaction proceeded at 90 °C for 7 d. The reaction mixture appears a dark brown (monomer **2**, **7**) or dark green (monomer **6**) color. Upon reaction termination, a solution of 5 mass % HCl in methanol was added to quench the zinc metal. After concentrating the resulting mixture, the polymer was precipitated in water. It was then redissolved and subjected to dialysis for lithium ion exchange. The final product was achieved by completely removing solvent at 180 °C in a vacuum oven for 24 h.

Poly-6

Yield: 0.98 g (63.2%).

^{1}H NMR (400 MHz, DMSO-d_6) δ 8.10–6.70 (m, 3H), 4.41–3.81 (m, 2H), 3.03–2.80 (m, 2H), 1.95–1.06 (m, 16H).

ATR-FTIR (ZnSe; cm^{-1}): 2926, 2856, 1603, 1468, 1385, 1187, 1118, 1064, 811, 717.

Found: Li 1.52% (calc. 1.54%).

Poly-7

Yield: 0.91 g (49.8%).

^{1}H NMR (400 MHz, DMSO-d_6) δ 7.94–6.79 (m, 8H), 4.28–3.82 (m, 2H), 2.93–2.72 (m, 2H), 1.92–0.97 (m, 16H).

ATR-FTIR (ZnSe; cm^{-1}): 2922, 2852, 1602, 1467, 1386, 1119, 1086, 1067, 809, 723.

Found: Li 1.44% (calc. 1.51%).

Oligo-2

Yield: 0.67 g (48.5%).

^{1}H NMR (400 MHz, DMSO-d_6) δ 7.92–6.73 (m, 3H), 4.38–3.78 (m, 2H), 2.40 (m, 2H), 1.90–0.93 (m, 16H).

ATR-FTIR (ZnSe; cm^{-1}): 2920, 2851, 1601, 1467, 1385, 1175, 1061, 800, 722.

Found: Li 2.10% (calc. 2.17%).

Results and discussion

Polymer synthesis and macromolecular design

In our study, we employ the non-polar and *para*-positioned polyphenylene backbone. Alkyl segments with ten –CH$_2$– groups were used as spacer groups between the polymer backbone and tethered anion, which affords the anion some flexibility and configurational freedom. Other works have shown that polymers with alkyl side-chains exhibit nanoscale phase segregation and side chain dynamics that are separated from that of the main chain.[30] In the case of termination of the side-chain with an ionic group, an ion-rich phase separate from the main chain may form. Here, the chemistry of the tethered anion at the end of the side-chain is altered to change the local environment of the lithium cation. The sulfonate anion (–SO$_3^-$), commonly found in many commercialized ionomers, has the smallest size compared to the other two anions in our study, which gives it the highest electrostatic attraction to Li$^+$.[31] The sulfonyl(trifluoromethylsulfonyl)imide (–TFSI$^-$) functionality presents additional electron-withdrawing components which allows for the highest charge delocalization of the three anions. Polymer electrolytes containing –TFSI$^-$ derivatives have been widely studied for use in Li-ion and Li metal batteries and exhibit sufficient electrochemical stability. Finally, we prepare a polymer with a sulfonylphenylsulfonylimide (–PSI$^-$)-based anion where the phenyl ring replaces the trifluoromethane group of the –TFSI$^-$. This –PSI$^-$ anion should have reduced charge delocalization compared to the –TFSI$^-$, but a significantly higher charge delocalization when compared to –SO$_3^-$ (–SO$_3^-$ ≪ –PSI$^-$ < –TFSI$^-$).

The synthesis procedures for sulfonate anion modifications on vinyl monomers have been discussed extensively by Shaplov and colleagues starting from the sulfonyl chlorination step.[32] In our study, the stable dichlorophenyl polymerizable moiety eliminates the oligo/polymerization of the intermediate compounds. Scheme 1 shows the synthesis of the –SO$_3^-$, –TFSI$^-$, and –PSI$^-$ monomers and their corresponding polymers (oligo-2, poly-6, and poly-7, respectively). Each polymer was synthesized *via* the Negishi coupling reaction.[33] The structural details of the polymers can be found in Table 1 and characterization data for intermediates and final products, as
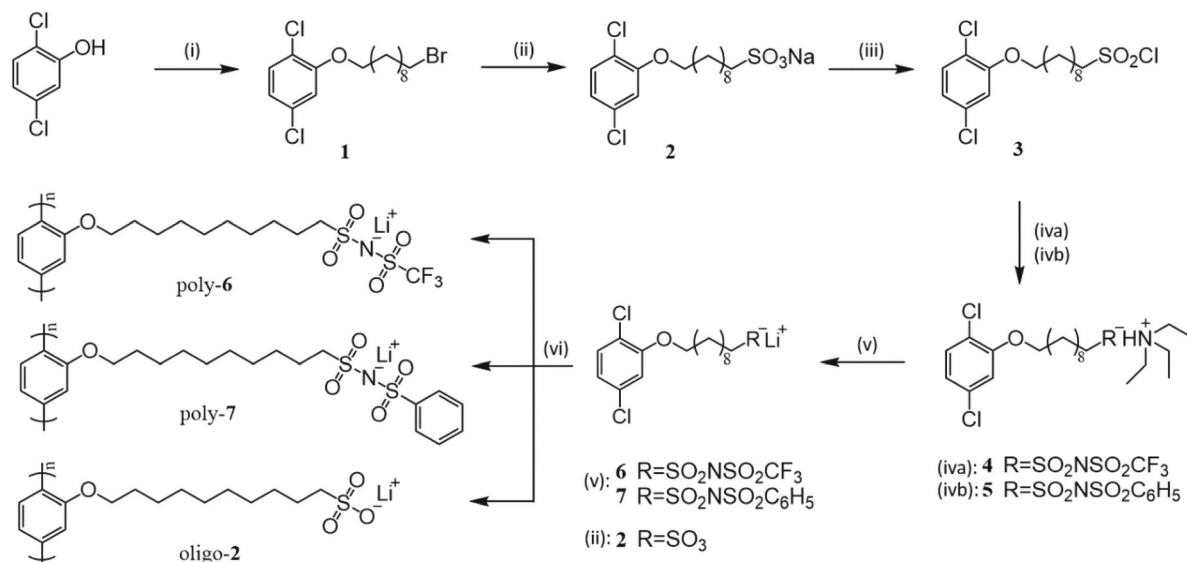
Scheme 1 Synthesis route for poly-6, poly-7, and oligo-2. (i) 1,10-dibromodecane, K$_2$CO$_3$, KI, acetone, reflux; (ii) Na$_2$SO$_3$, BzNEt$_3$Br, ethanol/water, reflux; (iii) SOCl$_2$, DMF (cat.), THF, 0 °C – r.t. (room temperature); (iva/b) H$_2$NSO$_2$CF$_3$/H$_2$NSO$_2$C$_6$H$_5$, triethylamine, THF, 0 °C – r.t.; (v) LiH, THF, 0 °C – r.t.; (vi) NiCl$_2$, P(Ph)$_3$, bpy, zinc, DMAc, 90 °C, dialysis.

Table 1 Structural details of polymers, including number averaged molecular mass (M_n, Da; analyzed in mobile phase: [a]DMF, [b]ACN/H_2O) and dispersity ($Đ$)

| Sample	Anion	M_n (Da)	$Đ$
poly-6	−TFSI$^-$	8000[a]	2.37
poly-7	−PSI$^-$	7400[a]	1.51
oligo-2	−SO$_3$$^-$	1400[b]	1.57

well as discussion of the synthetic route, may be found in the ESI.† Polymer molar masses are on par with what has been observed previously for Negishi polymerization of similar non-ionic monomers.[34] The ^{1}H NMR of the three polymers are displayed in Fig. 1. The characteristic peaks in the aromatic region as well as the aliphatic proton (δ 4.41–3.81, Fig. 1, labeled a) and the −SO$_2$− adjacent proton are broadened which indicates the polymerization/oligomerization of the mono-mers. The −SO$_2$− adjacent proton peak (Fig. 1, labeled b) shifts systematically from high to low field as the charge-delocalizing nature of −TFSI$^-$ (δ 2.92), −PSI$^-$ (δ 2.84), and −SO$_3$$^-$ (δ 2.40) decreases.

Thermal behavior

Since ion-transport properties in PILs and polar single-ion conducting polymer electrolytes are partially influenced by segmental chain flexibility, differential scanning calorimetry

(DSC) was used to determine the glass transition temperatures of the polymers/oligomer. The DSC profiles for poly-6, poly-7, and oligo-2 are displayed in Fig. 2 for the temperature range of 50 °C to 200 °C; full cooling and heating scans are displayed in the ESI as Fig. S17, S18, and S19.† There is no thermal transition found in this range for oligo-2, but an exothermic peak
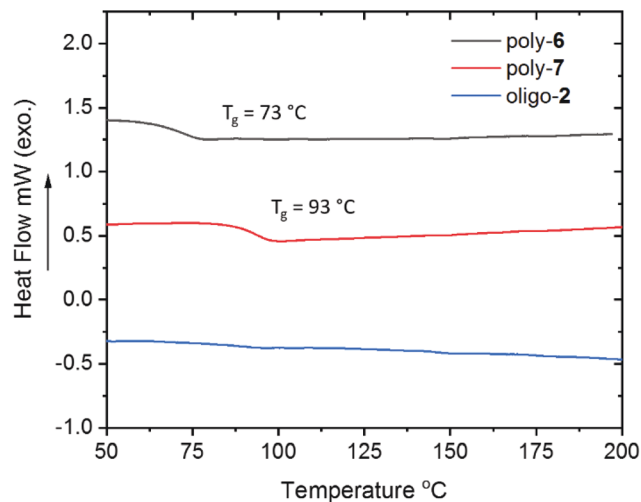
Fig. 2 DSC thermograms of poly-6, poly-7, and oligo-2 at 10 °C min^{-1} heating rate.
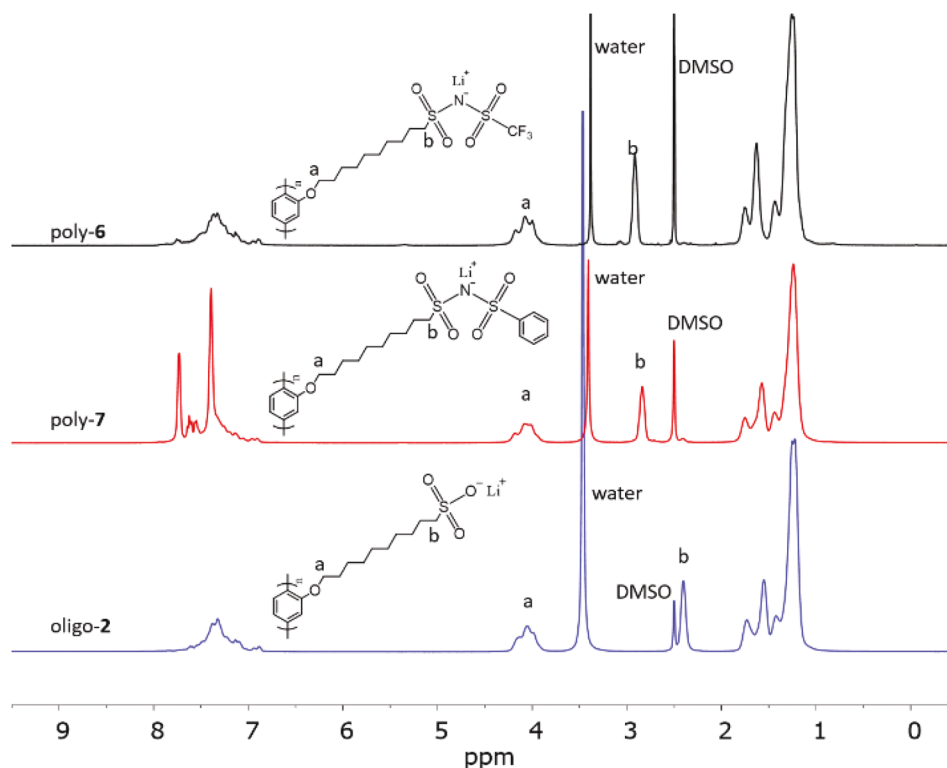
Fig. 1 ^{1}H NMR spectrum of poly-6 (black), poly-7 (red), and oligo-2 (blue) in DMSO-d_6. Note the key protons on methylene groups identified as (a) adjacent to the oxygen atom and (b) adjacent to the sulfur atom, as shown on the structural diagrams.

is present at 289 °C which is ascribed to melting of the ionic phase. Thermal gravimetric analysis (TGA) of oligo-**2** is displayed in the ESI as Fig. S20† which indicates that this transition is concomitant with decomposition. For poly-**6** and poly-**7**, no melting transitions are observed, and a single glass transition is found for each polymer at 73 °C and 93 °C, respectively. These two glass transition temperatures are greater than those typically observed for PILs, because the Li$^+$ has a higher charge density than an organic cation.[35–37] Two glass transition temperatures are often observed for alkyl side-chain polymers, one transition by the main chains and one transition by the side-chains, and for high molecular mass *para*-polyphenylene, the T_g has been reported to be 185 °C.[30,38] We hypothesize that in this case a single glass transition exists due to the lower overall molecular mass and plasticizing effect of the side groups. In contrast to the –TFSI$^-$, the –PSI$^-$ group possesses greater bulkiness and interaction with Li$^+$. Thus, the higher T_g was found for the –PSI$^-$ polymer. In comparison, the T_g of LiPSTFSI was measured to be 256 °C, being different than previously reported values, which is potentially due to higher absolute molecular weight (Fig. S21†).[19]

Ionic conductivity

As the polymer bulk diffusion is orders of magnitude slower than the mobile counter-ion, lithiated ionomers containing PEO components usually show a transference number greater than 0.9.[6] In this study, anion groups are also fixed on the polymer backbone. Hence, the conductivity measured by dielectric spectroscopy is essentially from Li$^+$ motion and the contribution from anion transport is considered to be negligible. The temperature dependent conductivity of polymeric ion conductors consists of two typical modes: (1) Arrhenius behavior which results from ion hopping in a glassy or crystalline matrix, or (2) Vogel–Fulcher–Tammann (VFT) behavior that results from ion transport coupled with chain relaxation dynamics.[39] The conductivity as a function of temperature for the three newly synthesized polymer as well as the more common LiPSTFSI is displayed in Fig. 3. Significant differences in the ion transport rate and temperature dependence are immediately obvious. The highest conductivity was achieved by poly-**6** at 6.7×10^{-6} S cm^{-1}, 1.1×10^{-8} S cm^{-1}, and 5.6×10^{-12} S cm^{-1} for 150 °C, 90 °C, and 60 °C, respectively. We note that these conductivity values are lower than that of a typical PEO-based solid state electrolyte by several orders of magnitude. However, the phenomena that lead to the significant differences in ion transport properties between the materials studied here are investigated to provide insight to how one may design new, efficient single-ion conductors without polar matrices.

It is observed that the LiPSTFSI presented an Arrhenius behavior up to the higher end measurement temperature of 180 °C. This is a result of the rigid polystyrene backbone and the added dense electrostatic attractions provided by the direct attachment of ionic groups to the *para*-styrene position. Instead, the VFT behavior was found for both poly-**6** and poly-
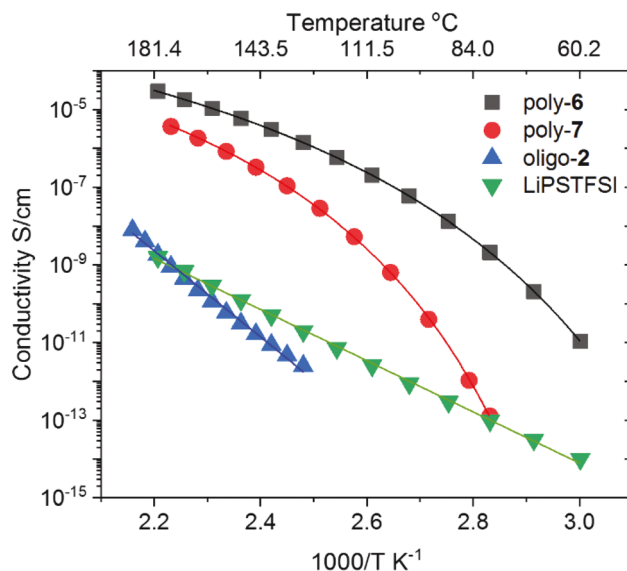

Fig. 3 Conductivity spectra. Lines show fits to VFT behavior for poly-**6** and poly-**7** and Arrhenius behavior for oligo-**2** and LiPSTFSI.

7 throughout the temperature range being measured. These side-chain polymers demonstrated appreciably higher ionic conductivity ($\approx$3 to 4 orders of magnitude higher) with the same and similar tethered anion chemistry to LiPSTFSI. We noted that the *p*-polyphenylene backbone presents minimal flexibility due to its 180° bond angle, which results in higher backbone rigidity than the polystyrene. However, in our polymers, the ten flexible carbon spacers were enough to provide the side-chain terminal ionic groups with configurational freedom and enhanced dynamics.

The effect of the anion chemistry on the conductivity is also evident. As shown in Fig. 3, oligo-**2** has the lowest conductivity, likely due to the strong interaction between –SO$_3^-$ and Li$^+$ that results in a crystalline ionic phase. The poly-**7** displayed conductivities of 8.3×10^{-7} S cm^{-1} and 3.9×10^{-11} S cm^{-1} at 150 °C and 90 °C, respectively, which are significantly lower than those of the poly-**6** sample. Comparing to the –TFSI$^-$ anion, the –PSI$^-$ anion possesses decreased charge delocalization. The increase in binding affinity may slow the cation hopping within the ionic aggregate and/or slow the side-chain relaxation dynamics. The larger size of the –PSI$^-$ anion may also slow chain end relaxation dynamics. The ionic conductivity in this type of polymer electrolyte is acutely sensitive to anion chemistry.

Ion transport mechanism

To investigate the mechanism of ion transport in these side-chain polymer electrolytes, we applied dielectric relaxation analysis in the frequency domain. Only poly-**6** and poly-**7** were subjected to analysis because the oligo-**2** and LiPSTFSI were in the crystalline and glassy states, respectively, at the measurement temperatures. A representative dielectric analysis spectrum of poly-**6** at 90 °C is displayed in Fig. 4. The dielectric
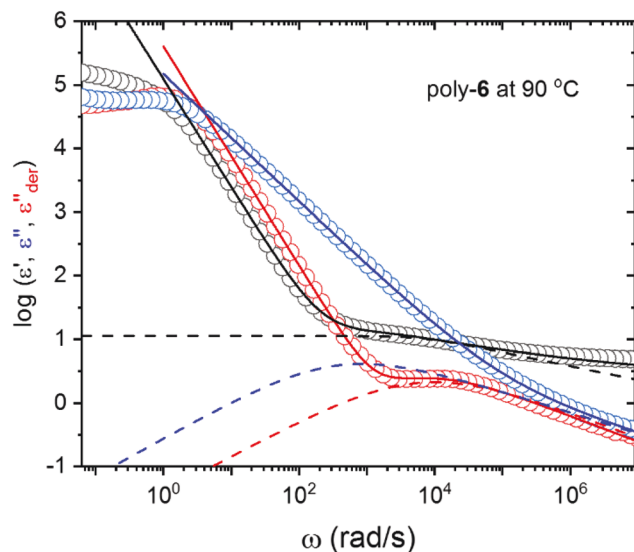
Fig. 4 Dielectric constant (black), dielectric loss (blue), and derivative dielectric loss (red) spectra are shown in open symbols for poly-**6** at 90 °C, along with results of fitting of the spectra to eqn (2) (solid line) and the contribution of the HN relaxation process (dashed line).

constant (ε') and dielectric loss (ε'') are presented, as well as the dielectric loss derivative (ε''_{der}) which was derived from Kronig–Kramers relationship:[40]

$$\varepsilon''_{der}(\omega) = -\frac{\pi}{2}\frac{\partial \varepsilon'(\omega)}{\partial \ln \omega} \tag{1}$$

In the high frequency region, the ε' spectrum contains a moderate slope which is related to the dielectric relaxation process. In the middle frequency region, the spectrum displays a sharp rise which is due to the electrode polarization (EP) by the blocking electrode. The EP region at low frequency is manifested by a plateau. The ε'' spectrum provides limited information because the ion transport signal buries that from the relaxation process. From the analysis of the ε''_{der} spectrum, which eliminates the ion transport signal, it was found that there is one loss peak at the medium to high frequency region overlapping with the EP take-off. Considering that the poly-**6** and poly-**7** backbone is extremely rigid and the aryl–alkyl ether group has low polarity, we thus decided to fit to the one-term Havriliak–Negami (HN) function plus one ion transport term and one EP term to analyze the dielectric relaxation process:[41]

$$\varepsilon^* = \varepsilon' - \mathbf{i}\varepsilon'' = \varepsilon_\infty + \frac{\Delta\varepsilon}{[1 + (\mathbf{i}\tau_{HN}\omega)^\alpha]^\beta} + \frac{\mathbf{i}\sigma}{\varepsilon_0\omega} + A\omega^{-S} \tag{2}$$

wherein α and β are two shape parameters, $\Delta\varepsilon$ is the dielectric relaxation strength, τ_{HN} is HN relaxation time, ε_0 is vacuum permittivity, ε_∞ is the dielectric constant at infinite high frequency, σ is the conductivity, and A and S are two constants. From the characteristic HN relaxation time, the

maximum dielectric relaxation time (τ_{max}) can be obtained as follows:

$$\tau_{max} = \tau_{HN}\left(\sin\frac{\alpha\beta\pi}{2+2\beta}\right)^{1/\alpha}\left(\sin\frac{\alpha\pi}{2+2\beta}\right)^{-1/\alpha} \tag{3}$$

As it is presented in Fig. 5, the maximum relaxation frequency (ω_{max}), which is the inverse of τ_{max}, is plotted *versus* inverse temperature for poly-**6** and poly-**7**. Both datasets are well fit by the VFT model. By extrapolating the curves to low frequency where the relaxation time is infinitely long, we obtain that the T_g by dielectric relaxation spectroscopy (DRS T_g) for poly-**6** is 47 °C and for poly-**7** is 75 °C. After scaling the temperature against the DRS T_g, the two relaxation frequency curves collapse on top of each other, indicating that the dielectric moment governs the relaxation processes (Fig. 5, inset). The DRS T_g is lower than the DSC T_g by $\Delta T_{g, DSC–DRS}$ = 26 °C and 18 °C for poly-**6** and poly-**7**, respectively. For typical PILs with flexible backbones, the DRS T_g is usually within a few degrees of the DSC T_g.[24,36,42] For polymers with pendent flexible chains, similar to our system, differences between main chain and side-chain dynamics are commonly observed.[23] We expect that the observed dielectric relaxation here is dominated by the polarizable side-chain (notably, the ionic group), and therefore we infer that the rigid *p*-phenylene backbone likely causes the difference between the DRS and DSC glass transitions temperatures. The observed DSC T_g is a weighted average from backbone and side-group contributions, while the DRS T_g is more heavily affected by relaxation of the side-chains, which are more dielectrically susceptible.

Fig. 6 shows the dielectric relaxation strength *versus* inverse temperature. The magnitude of the dielectric relaxation strength of the two polymers (poly-**6** and poly-**7**) is lower than
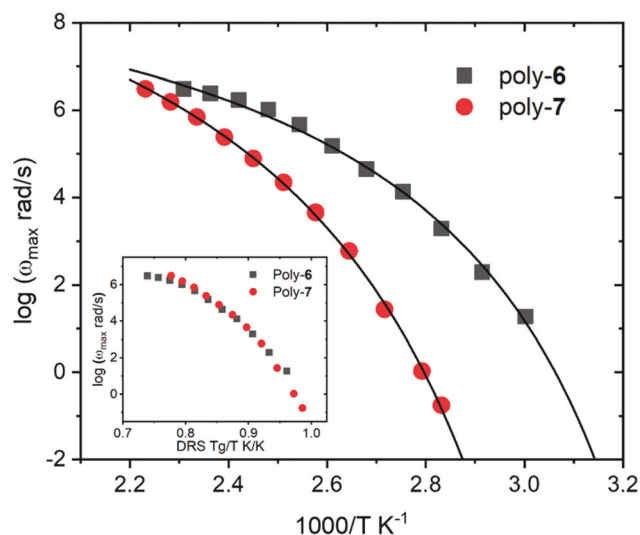
Fig. 5 Calculated maximum relaxation frequency (ω_{max}) of poly-**6** and poly-**7** which show VFT curves. The two curves are reduced to one common curve by normalizing the temperature against DRS T_g (inset). Lines show fits to the VFT equation. Standard errors are smaller than the size of the data points.
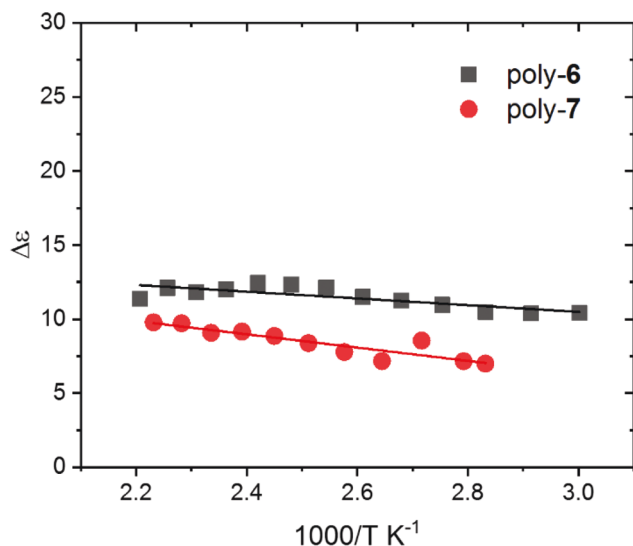
Fig. 6 Dielectric relaxation strength of poly-**6** and poly-**7**. Standard errors are less than 15%.

that for typical PILs with organic ion pairs (typical range from ≈40 to 200). This difference is a result of higher attraction between Li^{+} and the anions, as well as ion pair confinement from the rigid backbone.[24,25,36] Additionally, our polymers showed the same trend: the relaxation strength of poly-**6** and poly-**7** increase slightly as temperature increases. A decreased dielectric relaxation strength with increasing temperature is commonly found, in accordance with Onsager theory.[41] The attraction of each –TFSI[−] and –PSI[−] to Li^{+} is such that the separation of ionic pairs is more susceptible to thermal effects.

Temperature dependent ionic conductivity normalized by T_g is presented for poly-**6** and poly-**7** in Fig. 7, and conductivity normalized by DSC T_g is presented for LiPSTFSI as Fig. S22.† Scaling by the DSC T_g does not collapse the conductivity, which is usually observed in PIL materials where the counterion transport is dominated by matrix softness.[36] However, scaling by the DRS T_g reduces the data for poly-**6** and poly-**7** to a common curve. We thus can induce that the ion conduction is correlated to the dielectric relaxation and, likely, the tethered ionic group relaxation. For pure LiTFSI salt, Li^{+} is coordinated with four S═O oxygens of the anions.[43] Similar coordination environment is expected for poly-**6** and poly-**7**. In the electric field, the Li^{+} may transport within the aggregate between coordination sites *via* ionic cluster rearrangements. The dielectric relaxation observed is related to the dipole moment created during the rearrangement process; we hypothesize that the dynamics of these rearrangements are coupled to the anion group dynamics. The exact relationship between the dielectric relaxation and side-chain dynamics cannot yet be determined.

We further applied the universal correlation between conductivity and ionic relaxation, introduced by Barton, Nakajima, and Namikawa (BNN).[44–46] This correlation suggests that the dielectric relaxation and ion conduction share the same origin, according to which, an empirical relationship was established: $\sigma = B\varepsilon_0\varepsilon_s\omega_{max}$, where B is the universal scaling factor and ε_s (= $\Delta\varepsilon + \varepsilon_\infty$) is the static dielectric constant. For most previously reported glassy ion conductors, B was found to be equal to or greater than unity which indicates a strong correlation between ion conduction and dielectric relaxation. As it is displayed in Fig. 8, both poly-**6** and poly-**7** were scaled on the same line which has a B factor of ≈1. This further suggests that the Li^{+} transport is strongly coupled to the ionic group relaxation.
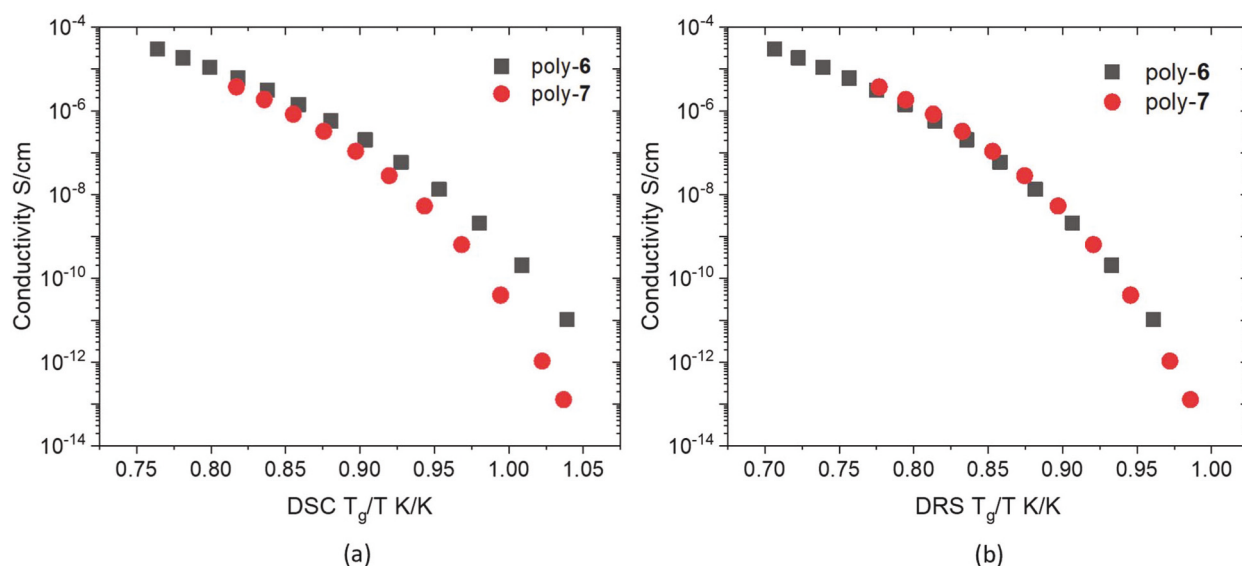

Fig. 7 (a) The conductivity curves of poly-**6** and poly-**7** *versus* temperature normalized by DSC T_g. (b) The conductivity curves of poly-**6** and poly-**7** *versus* temperature normalized by DRS T_g. A reduced common curve was found.
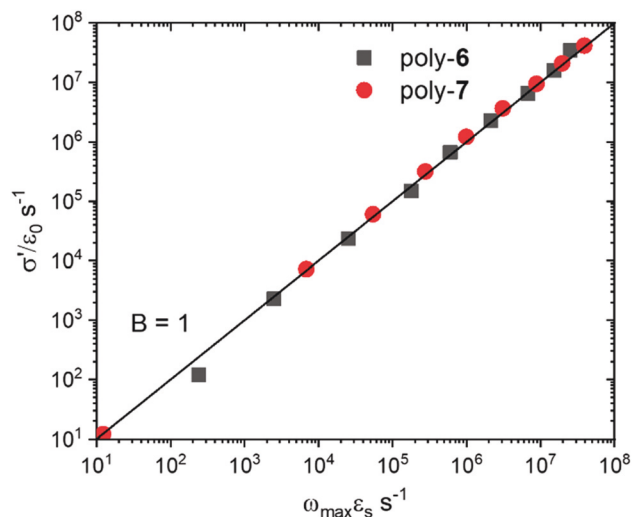
Fig. 8 The BNN plot of poly-**6** and poly-**7**. Both of the two materials show the universal scaling factor $B \approx 1$. Standard errors are smaller than the size of the data points.

Conclusions

In this contribution, we have successfully created a model side-chain single-ion conducting lithium polymer electrolyte through the Negishi coupling polymerization of anion functionalized p-phenylene monomers, with the added advantage of chemical stability of the monomer during anion group modification. By placing the ionic groups on side-chains, we are able to decouple the ion transport from the main chain dynamics. The physio-chemical properties of the anion groups were examined for their lithium-ion conduction efficiency, and we found that the conductivity of these polymer electrolytes is strongly dependent on the anion chemistry. We also observed that placement of the tethered anion group at the end of the side-chains allows for increased anion group dynamics, which correlates with improved ionic conductivity. The DRS T_g (but not the DSC T_g) is related to ion transport, as is indicated by the temperature scaled common conductivity curve. Furthermore, BNN scaling theory analysis indicates that the ion transport is strongly coupled to dielectric relaxation. These findings suggest that faster ion transport may be achievable through engineering of the conducting ion local environment and without sacrificing mechanical properties. We are examining the amenability of this phenomenon for other rigid backbone polymers and further investigation of the effects of side-chain length, backbone flexibility, and morphology of these types of single-ion conducting polymer electrolytes is ongoing. With increased active ion conductivities, solvent-free single-ion conducting polymer electrolytes have potential for enabling safe, high energy, and high performing energy storage technologies.

Conflicts of interest

There are no conflicts of interest to report.

Acknowledgements

Notes and references

1 M. Li, J. Lu, Z. Chen and K. Amine, *Adv. Mater.*, 2018, **30**, 1800561.
2 J.-M. Tarascon and M. Armand, *Nature*, 2001, **414**, 359–367.
3 J. B. Goodenough and K. S. Park, *J. Am. Chem. Soc.*, 2013, **135**, 1167–1176.
4 Z. Xue, D. He and X. Xie, *J. Mater. Chem. A*, 2015, **3**, 19218–19253.
5 X.-G. Sun and J. B. Kerr, *Macromolecules*, 2006, **39**, 362–372.
6 H. Zhang, C. Li, M. Piszcz, E. Coya, T. Rojo, L. M. Rodriguez-Martinez, M. Armand and Z. Zhou, *Chem. Soc. Rev.*, 2017, **46**, 797–815.
7 M. Doyle and J. Newman, *J. Appl. Electrochem.*, 1997, **27**, 846–856.
8 S. M. R. Bouchet, R. Meziane, A. Aboulaich, L. Lienafa, J.-P. Bonnet, T. N. T. Phan, D. Bertin, D. Gigmes, D. Devaux, R. Denoyel and M. Armand, *Nat. Mater.*, 2013, **12**, 452–457.
9 H. Zhang, C. Liu, L. Zheng, F. Xu, W. Feng, H. Li, X. Huang, M. Armand, J. Nie and Z. Zhou, *Electrochim. Acta*, 2014, **133**, 529–538.
10 Q. Ma, H. Zhang, C. Zhou, L. Zheng, P. Cheng, J. Nie, W. Feng, Y. S. Hu, H. Li, X. Huang, L. Chen, M. Armand and Z. Zhou, *Angew. Chem., Int. Ed.*, 2016, **55**, 2521–2525.
11 S. Feng, D. Shi, F. Liu, L. Zheng, J. Nie, W. Feng, X. Huang, M. Armand and Z. Zhou, *Electrochim. Acta*, 2013, **93**, 254–263.
12 X. Chen, F. Chen, M. S. Liu and M. Forsyth, *Solid State Ionics*, 2016, **288**, 271–276.
13 R. Meziane, J.-P. Bonnet, M. Courty, K. Djellab and M. Armand, *Electrochim. Acta*, 2011, **57**, 14–19.
14 M. Singh, O. Odusanya, G. M. Wilmes, H. B. Eitouni, E. D. Gomez, A. J. Patel, V. L. Chen, M. J. Park, P. Fragouli, H. Iatrou, N. Hadjichristidis, D. Cookson and N. P. Balsara, *Macromolecules*, 2007, **40**, 4578–4585.
15 A. Panday, S. Mullin, E. D. Gomez, N. Wanakule, V. L. Chen, A. Hexemer, J. Pople and N. P. Balsara, *Macromolecules*, 2009, **42**, 4632–4637.
16 B. P. Kirkmeyer, A. Taubert, J.-S. Kim and K. I. Winey, *Macromolecules*, 2002, **35**, 2648–2653.
17 E. B. Trigg, L. R. Middleton, L. Yan and K. I. Winey, *Macromolecules*, 2018, **51**, 7942–7950.
18 L. R. Middleton, E. B. Trigg, L. Yan and K. I. Winey, *Polymer*, 2018, **144**, 184–191.

19 P.-F. Cao, Z. Wojnarowska, T. Hong, B. Carroll, B. Li, H. Feng, L. Parsons, W. Wang, B. S. Lokitz, S. Cheng, V. Bocharova, A. P. Sokolov and T. Saito, *Polymer*, 2017, **124**, 117–127.

20 D. S. Bolintineanu, M. J. Stevens and A. L. Frischknecht, *ACS Macro Lett.*, 2013, **2**, 206–210.

21 L. M. Hall, M. J. Stevens and A. L. Frischknecht, *Macromolecules*, 2012, **45**, 8097–8108.

22 L. Yan, M. Häußler, J. Bauer, S. Mecking and K. I. Winey, *Macromolecules*, 2019, **52**, 4949–4956.

23 D. Mecerreyes, *Prog. Polym. Sci.*, 2011, **36**, 1629–1648.

24 U. H. Choi, A. Mittal, T. L. Price, H. W. Gibson, J. Runt and R. H. Colby, *Macromolecules*, 2013, **46**, 1175–1186.

25 S. Liang, U. H. Choi, W. Liu, J. Runt and R. H. Colby, *Chem. Mater.*, 2012, **24**, 2316–2323.

26 Z. Wojnarowska, H. Feng, Y. Fu, S. Cheng, B. Carroll, R. Kumar, V. N. Novikov, A. M. Kisliuk, T. Saito, N.-G. Kang, J. W. Mays, A. P. Sokolov and V. Bocharova, *Macromolecules*, 2017, **50**, 6710–6721.

27 J. R. Sangoro, C. Iacob, A. L. Agapov, Y. Wang, S. Berdzinski, H. Rexhausen, V. Strehmel, C. Friedrich, A. P. Sokolov and F. Kremer, *Soft Matter*, 2014, **10**, 3536–3540.

28 Y. Cheng, J. Yang, J.-H. Hung, T. K. Patra and D. S. Simmons, *Macromolecules*, 2018, **51**, 6630–6644.

29 A. K. Jonscher, *J. Phys. D: Appl. Phys.*, 1999, **32**, R57–R70.

30 M. Beiner and H. Huth, *Nat. Mater.*, 2003, **2**, 595–599.

31 K. A. Mauritz and R. B. Moore, *Chem. Rev.*, 2004, **104**, 4535–4586.

32 A. S. Shaplov, P. S. Vlasov, M. Armand, E. I. Lozinskaya, D. O. Ponkratov, I. A. Malyshkina, F. Vidal, O. V. Okatova, G. M. Pavlov, C. Wandrey, I. A. Godovikov and Y. S. Vygodskii, *Polym. Chem.*, 2011, **2**, 2609–2618.

33 Y. Li, T. Yasuda, K. Miyatake and M. Watanabe, *Macromol. Chem. Phys.*, 2005, **206**, 2390–2395.

34 Y. Yang, Q. Pei and A. J. Heeger, *J. Appl. Phys.*, 1996, **79**, 934–939.

35 F. Frenzel, R. Guterman, A. M. Anton, J. Yuan and F. Kremer, *Macromolecules*, 2017, **50**, 4022–4029.

36 U. H. Choi, M. Lee, S. Wang, W. Liu, K. I. Winey, H. W. Gibson and R. H. Colby, *Macromolecules*, 2012, **45**, 3974–3985.

37 F. Fan, Y. Wang, T. Hong, M. F. Heres, T. Saito and A. P. Sokolov, *Macromolecules*, 2015, **48**, 4461–4470.

38 D. G. H. Ballard, A. Courtis, I. M. Shirley and S. C. Taylor, *Macromolecules*, 1988, **21**, 294–304.

39 S. B. Aziz, T. J. Woo, M. F. Z. Kadir and H. M. Ahmed, *J. Sci.: Adv. Mater. Dev.*, 2018, **3**, 1–17.

40 M. Wübbenhorst and J. v. Turnhout, *J. Non-Cryst. Solids*, 2002, **305**, 40–49.

41 F. Kremer and A. Schönhals, *Broadband Dielectric Spectroscopy*, Springer, Berilin, 2002.

42 F. Fan, W. Wang, A. P. Holt, H. Feng, D. Uhrig, X. Lu, T. Hong, Y. Wang, N.-G. Kang, J. Mays and A. P. Sokolov, *Macromolecules*, 2016, **49**, 4557–4570.

43 W. A. Henderson, D. M. Seo, Q. Zhou, P. D. Boyle, J.-H. Shin, H. C. De Long, P. C. Trulove and S. Passerini, *Adv. Energy Mater.*, 2012, **2**, 1343–1350.

44 H. Namikawa, *J. Non-Cryst. Solids*, 1974, **14**, 88–100.

45 H. Namikawa, *J. Non-Cryst. Solids*, 1975, **18**, 173–195.

46 J. R. Macdonald, *J. Appl. Phys.*, 2010, **107**, 101101.